



Available online at www.sciencedirect.com

ScienceDirect

Comput. Methods Appl. Mech. Engrg. 386 (2021) 114084

Computer methods in applied mechanics and engineering

www.elsevier.com/locate/cma

A hybrid potential of mean force approach for simulation of fracture in heterogeneous media

Xuejing Wang^a, Meshkat Botshekan^b, Franz-Josef Ulm^b, Mazdak Tootkaboni^a, Arghavan Louhghalam^a,**

^a Department of Civil and Environmental Engineering, University of Massachusetts, Dartmouth, MA, USA
^b Department of Civil and Environmental Engineering, Massachusetts Institute of Technology, Cambridge, MA, USA

Received 24 March 2021; received in revised form 30 June 2021; accepted 30 July 2021

Available online xxxx

Abstract

Material heterogeneity at small scales is a key driver of material's effective macroscopic properties and fracture response. We present a hybrid energy-based approach based on a potential of mean force formulation of lattice element method for reliable and efficient modeling of fracture and crack propagation in heterogeneous materials. The proposed framework rests on direct application of the Griffith fracture criteria and removes material points to create fracture surfaces in energetically favorable directions. Computational efficiency is achieved through a probing of high energy bonds and quasi-static relaxation leading to near global imposition of the energy-based criteria for crack path resolution. We validate the proposed hybrid approach against results in literature and use it to examine fracture response of defective and layered materials. For layered materials with fracture energy heterogeneity, the effective toughness is shown to be the maximum of fracture energies of layers irrespective of their volume fraction and the direction of crack propagation. For layered materials with elastic modulus heterogeneity, the maximum energy release rate occurs when the crack approaches the compliant-stiff interface from within the compliant phase. We examine the scaling of fracture toughness with modulus contrast, the link to volume fraction of the layers and the relationship between toughness anisotropy and the gradient of elastic modulus heterogeneity, offering insights with potential to inform the design of materials for fracture.

© 2021 Elsevier B.V. All rights reserved.

Keywords: Potential of mean force; Lattice element method; Fracture of heterogeneous materials; Energy methods; Griffith fracture criteria; Energy release rate

1. Introduction

The impact of texture and structure at small scales on the effective macroscopic properties of heterogeneous materials has been subject of extensive research [1–5]. While well-established homogenization techniques relate the micro-structural characteristics to effective elastic properties [6–8], the relationship to fracture properties has not been thoroughly established yet [9]. This is largely due to the complexities that arise from the interaction of the discontinuities with each other and other present inhomogeneities, which cannot be captured through mean-field approaches.

E-mail address: alouhghalam@umassd.edu (A. Louhghalam).

^{*} Corresponding author.

Theoretical developments have mostly focused on the fracture properties of domains with simple pre-existing discontinuities, cracks and inclusions [10–16]. These developments become inapplicable when complex material microstructure and its impact on effective macroscopic properties and nonlinear response is of interest. Numerical approaches such as finite element analysis have been extensively used to solve the corresponding boundary value problems numerically in the continuum domain [17–21]. These methods, however, require mesh refinement around discontinuities to conform to the crack geometry during crack propagation [22,23]. While more advanced methods such as extended and embedded finite element methods minimize the demand for re-meshing around discontinuities and complex morphologies [24–33] challenges still remain in modeling dynamic fracture and fragmentation due to inherently discrete nature of the phenomenon [34,35].

With the growing interest in studying failure and fracture of heterogeneous materials at micro and meso scales, discrete methods have become increasingly popular due to their robustness in modeling discontinuities [36–41]. Lattice element models (LEM) constitute a class of discrete methods with great promise in modeling fracture and crack propagation in quasi-brittle materials [4,42–44] and interaction and coalescence of discontinuities in heterogeneous materials [45]. Since the introduction of lattice discretization in materials modeling [46], the idea and its application to study the behavior of heterogeneous materials has taken many forms [47]. Material domain is discretized to points that are connected by one dimensional central force, bending and shear elements [48,49] and fracture is modeled by breakage of bonds between the material points. This is commonly achieved via a strength- or strain-based criterion that utilizes a combination of force and moments to specify a bond breakage rule [36,50–52]. Fracture, however, as Griffith's postulates [53] is rather an energetically-driven phenomenon and is viewed as an irreversible process of energy release between a sequence of thermodynamic equilibrium states due to breakage of bonds and creation of new crack surfaces:

$$\mathcal{G} \le \mathcal{G}_c, \quad d\Gamma \ge 0, \quad (\mathcal{G} - \mathcal{G}_c)d\Gamma = 0$$
 (1)

with Γ the fracture surface, \mathcal{G}_c fracture energy of the material and \mathcal{G} potential energy release rate given by:

$$\mathscr{G} = -\frac{\partial \Pi}{\partial \Gamma} \tag{2}$$

This energy-based nature of fracture can be accounted for via a potential-of-mean-force (PMF) formulation. Similar to the methods widely used in soft-matter physics, the PMF approach starts with the discretization of the continuous medium into masses interacting through effective potentials, leading to interaction forces and moments. Unlike the traditional strength-based approaches to LEM, however, the PMF formulation enables the use of energy-based Griffith criteria in modeling both linear and nonlinear fracture mechanics [54].

To fully enforce the Griffith's fracture criteria, a global search is performed to identify the material points which, if removed, would lead to greatest energy release rate. The removal of a material point, however, is not to mean mass removal; rather it is merely a proxy for breakage of the bonds connected to a point in the discretized domain. While this approach has shown great promise in direct application of energy-based fracture criterion, it requires substantial computational power and becomes infeasible when modeling highly heterogeneous materials [54]. A local approach based on Irwin fracture criteria and removal of critical bonds at the crack tip on the other hand provides a more computationally viable alternative. The local approach, however, does not directly account for Griffith fracture criterion and suffers from implementation intricacies related to use of certain lattice types and calculation of fracture surfaces. In this work a novel hybrid approach for simulating fracture of heterogeneous materials is proposed. The proposed approach is different from the current LEM based approaches in that it enables near global imposition of the Griffith criteria while substantially reducing the computational cost associated with the global search. This is done through a probing of bonds' energies that allows for the identification of sites with the highest potential to impact the process of energy release and relaxation. The organization of the paper is as follows: We first review the PMF approach to LEM for modeling elastic response and describe the local and global approaches for modeling fracture (Section 2). In Section 3 we provide the details of the proposed hybrid approach. This includes the probing of high energy bonds and relaxation, and an analysis of computational cost and validation in Sections 3.1–3.3, as well as an examination of size effect in Section 3.4 and the link to local and global approaches in Section 3.5. Section 4 is devoted to the application to non-homogeneous media. This includes observations on the impact of toughness and elastic modulus heterogeneity, volume fraction as well as the link between modulus heterogeneity gradient and toughness isotropy where we demonstrate how the proposed method provides a means for accurate prediction of crack trajectories, and modeling of simultaneous crack propagation (Sections 4.1-4.3). Finally, Section 5 provides the concluding remarks.

2. The PMF approach to LEM

2.1. The basics of LEM

The fundamental idea behind the potential of mean force approach to LEM is the lattice discretization of domain into material points that interact with each other via potentials similar to those used in atomic and meso-scales simulations [55,56]. The total energy of the system is written as the sum of ground state energy V_i , two- and three-body potentials (V_{ii} , V_{iik}) as well as higher-order interactions potentials:

$$V_{tot} = \sum_{i}^{N} V_{i}(\vec{x}_{i}) + \sum_{i,j}^{N} V_{ij}(\vec{x}_{i}, \vec{x}_{j}) + \sum_{i,j,k}^{N} V_{ijk}(\vec{x}_{i}, \vec{x}_{j}, \vec{x}_{k}) + \cdots$$
(3)

with \vec{x}_i , \vec{x}_j , and \vec{x}_k the position vectors of material points i, j and k. Alternatively, consistent with the traditional formulation of LEM the two- and three-body interaction potentials can be replaced by stretch $V_{ij}^{\rm n}((\vec{x}_j - \vec{x}_i).\vec{e}_{\rm n})$ and bending potentials $V_{ij}^{\rm b}((\vec{x}_j - \vec{x}_i).\vec{e}_{\rm b}; (\vec{x}_j - \vec{x}_i).\vec{e}_{\rm t}; (\vec{\vartheta}_j - \vec{\vartheta}_i)$ [49,57], with $\vec{e}_{\rm n}$, $\vec{e}_{\rm b}$, $\vec{e}_{\rm t}$ the unit vectors in the local lattice frame, and $\vec{\vartheta}_i$, $\vec{\vartheta}_j$ the rotations at nodes i and j. Disregarding the shear and torsional actions, this representation is equivalent to assuming material points interact only with their immediate neighbors through axial and bending actions (see Fig. 1) and expressing the bond energy as:

$$V_{ij} = -\epsilon_0 + \left(V_{ij}^{\text{n}} + V_{ij}^{\text{b}}\right) \tag{4}$$

with ϵ_0 the well depth of the potential in undeformed configuration. The PMF approach opens the door to using different interaction potentials from harmonic potentials to a variety of non-harmonic potentials thereby allowing the modeling of both linear and nonlinear response. For harmonic potentials, for instance, the stretch and bending potentials in Eq. (4) are expressed in terms of the translational and rotational displacements $\vec{\delta}_i = \{\delta_i^{\rm n}, \delta_i^{\rm b}, \delta_i^{\rm t}\}$ and $\vec{\vartheta}_i = \{\vartheta_i^{\rm n}, \vartheta_i^{\rm b}, \vartheta_i^{\rm t}\}$ illustrated in Fig. 1(b). Letting $\vec{\lambda}_{ij} = (\vec{\delta}_j - \vec{\delta}_i)/\ell_0$ one can write:

$$V_{ij}^{n} = \frac{1}{2} \epsilon_{ij}^{n} \left(\lambda_{ij}^{n} \right)^{2}$$

$$V_{ij}^{b} = \frac{1}{2} \epsilon_{ij}^{t} \left\{ \left(\lambda_{ij}^{b} - \vartheta_{i}^{t} \right)^{2} + \left(\lambda_{ij}^{t} + \vartheta_{i}^{b} \right)^{2} + \left(\lambda_{ij}^{b} - \vartheta_{i}^{t} \right) \left(\vartheta_{i}^{t} - \vartheta_{j}^{t} \right) + \left(\lambda_{ij}^{t} - \vartheta_{i}^{b} \right) \left(\vartheta_{j}^{b} - \vartheta_{i}^{b} \right) \right.$$

$$\left. + \frac{1}{3} \left(\left(\vartheta_{j}^{b} - \vartheta_{i}^{b} \right)^{2} + \left(\vartheta_{i}^{t} - \vartheta_{j}^{t} \right)^{2} \right) \right\}$$

$$(5)$$

with ϵ_{ij}^n and ϵ_{ij}^t the parameters of axial and transversal interaction potentials, and $l_{ij}^0 = |(\vec{r}_j - \vec{r}_i).\vec{e}_n|$ the initial length of bond i-j. The non-negative potential parameters for harmonic potentials representing the elastic properties can be obtained through a calibration procedure for regular cubic lattice illustrated in Fig. 1; see [58]. For isotropic materials with elastic modulus E and Poisson's ratio v, it can be shown that $\epsilon_{ij}^{n,t} = Ea_0^3 \mathcal{F}_d^{n,t}(v,n)$ with a_0 size of the lattice unit cell, n the level of discretization, and $\mathcal{F}_d(v,n)$ given in Table 1 for normal and tangential directions. The subscripts in \mathcal{F} denote the direction of interacting neighbors, where 1 and 2 indicate respectively the closest neighbor direction ($l_{ij}^0 = a_0$), and the direction of neighbors along the short ($l_{ij}^0 = \sqrt{2}a_0$) diagonal as shown in Fig. 1. Note that v = 1/3 and 1/4 lead to central force lattices in two and three dimensions respectively where the potential parameters corresponding to bending deformation are all zero. Using a regular lattice and subsequently a set of predefined potential parameters will enhance the computational efficiency. In our simulations, however, we allow for small irregularities in the discretization by perturbing the location of nodes from their original locations to mitigate the impact of discretization on the results when modeling homogeneous materials. These irregularities are kept in place even for the ultimate application of the framework to heterogeneous materials, where a regular mesh is not expected to negatively impact the results.

Evoking the theorem of minimum potential energy, the deformation field must minimize the potential energy of the entire system, i.e. $\Pi = V_{tot} - W$ with W the external work supplied to the system. Conjugate gradient (CG) methods such as Fletcher–Reeves–Polak–Ribiere (FRPR) method [59,60], are typically employed to minimize Π and obtain the translational and rotational displacements at each equilibrium state. The interacting forces and moments are the derivatives of the potential energy with respect to the translational and rotational deformation,

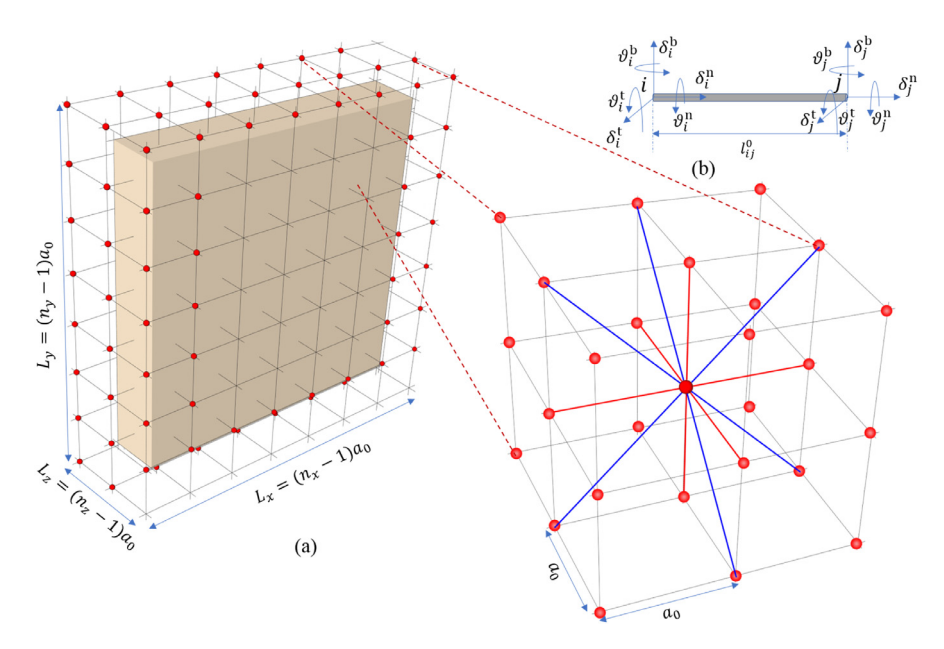


Fig. 1. (a) Material discretization in lattice element method (b) degrees of freedom in the bond's local coordinate system $(\vec{e}_n, \vec{e}_h, \vec{e}_t)$.

Table 1 The dimensionless calibration function $\mathcal{F}_d(\nu, n)$, after [58].

The dimensionless canonical ranction $\sigma_{\mathcal{U}}(v,n)$, area [50].				
Energy parameter	2D: $0 \le v \le 1/3$	2D: $-2/3 \le \nu \le 0$	3D: $0 \le \nu \le 1/4$	3D: $-1 \le v \le 0$
$\mathcal{F}_{\mathfrak{l}}^{\mathfrak{n}}$	$\frac{n(2-3\nu)-2(1-\nu)}{4n(1-\nu^2)}$	$\frac{n(2+3\nu)-2(1+\nu)}{4n(1-\nu^2)}$	$\frac{(n-1)^2(1-3\nu)}{n^2(1+\nu)(1-2\nu)}$	$\frac{(n-1)^2}{n^2(1-2\nu)}$
$\mathscr{F}_2^{\mathrm{n}}$	$\frac{\nu}{1-\nu^2}$	0	$\frac{2\nu(n-1)}{n(1+\nu)(1-2\nu)}$	0
\mathscr{F}^{t}_{l}	$\frac{(n-1)(1-3\nu)}{2n(1-\nu^2)}$	$\frac{(n-1+\nu)}{2n(1-\nu^2)}$	$\frac{(n-1)^2(1-4\nu)}{n^2(1+\nu)(1-2\nu)}$	$\frac{(n-1)^2}{n^2(1+\nu)(1-2\nu)}$
\mathscr{F}_2^{t}	0	$-\frac{\nu}{1-\nu^2}$	0	$-\frac{2\nu(n-1)}{n(1+\nu)(1-2\nu)}$

i.e. $\vec{F}_i^j = -\partial V_{ij}/\partial \vec{\delta}_i$ and $\vec{M}_i^j = -\partial V_{ij}/\partial \vec{\vartheta}_i$ and must satisfy the momentum balance:

$$\frac{\partial V_{ij}}{\partial \vec{\delta}_i} + \frac{\partial V_{ij}}{\partial \vec{\delta}_j} = \vec{0}; \qquad \frac{\partial V_{ij}}{\partial \vec{\vartheta}_i} + \frac{\partial V_{ij}}{\partial \vec{\vartheta}_j} + (\vec{x}_j - \vec{x}_i) \times \frac{\partial V_{ij}}{\partial \vec{\delta}_j} = \vec{0}$$
 (6)

The equivalent nodal stress tensor can then be obtained using virial representation once the forces are determined:

$$\sigma_i = \frac{1}{2v_i} \sum_{i=1}^m (\vec{x}_j - \vec{x}_i) \otimes \vec{F}_i^j \tag{7}$$

where v_i is the voxel volume centered at material point i, m is the number of neighboring material points, and \otimes represents the tensor product.

2.2. Modeling fracture: local and global views

In conventional LEM, fracture is modeled through breakage of bonds between two or more material points using strength-based failure criteria. These vary from maximum tensile stress or strain criterion to other classical failure criteria such as von-Mises [61–63]. However, from a thermodynamic perspective, fracture is an energetically irreversible process represented by a sequential bond breakage between two constrained equilibrium states in a quasistatic condition. Consistent with the PMF approach, once the relative position of material points reaches a limit, beyond which their interaction potentials do not contribute to the total potential energy of the system ($V_{ij} \rightarrow 0$), the bond between them is considered to be broken and the corresponding energy is dissipated leading to creation

of new fracture surface. Using Griffith fracture criteria:

$$\mathscr{E}_{ij} = -\frac{\Delta V_{ij}}{\Delta \Gamma_{ii}} = -\frac{V_{ij}(\vec{\lambda}_{ij}) - V_{ij}(\ell_0 \vec{e}_n)}{\Delta \Gamma_{ii}} \le -\frac{V_{ij}(\vec{\lambda}_{ij}^c) - V_{ij}(\ell_0 \vec{e}_n)}{\Delta \Gamma_{ii}} = \frac{\epsilon_0}{\Delta \Gamma_{ij}} = \mathscr{E}^b$$
(8)

with $\Delta\Gamma_{ij}$ the surface area created by bond breakage, and λ_{ij}^c the critical strain at fracture. In the above equation, $\epsilon_0/\Delta\Gamma_{ij}$ can be viewed as the fracture energy of the bond \mathcal{G}^b .

The local approach for modeling fracture utilizes the above criterion to obtain a critical force for bond fracture by obtaining the critical distance between two material points beyond which the bond potential is negligible. For a central force lattice, for instance, this is equivalent to $V_{ij}^{\rm n}(\lambda_c) = \epsilon_0$ (see Appendix for a more general relationship in presence of bending potential). Considering the harmonic potential:

$$V_{ij}^{\mathbf{n}} = -\epsilon_{ij}^{0} + \frac{\epsilon_{ij}^{\mathbf{n}}}{2} (\lambda_{ij}^{\mathbf{n}})^{2} \tag{9}$$

the normalized critical distance is $\lambda^c = \sqrt{2\epsilon_{ij}^n/\epsilon_{ij}^0}$ and the critical force corresponding to bond fracture $F_{i,c}^j = 1/l_{ij}^0 \sqrt{2\epsilon_{ij}^0 \epsilon_{ij}^n}$ is expressed in terms of bond elastic and fracture properties:

$$F_{i,c}^{j} = \frac{\sqrt{\Delta \Gamma_{ij}}}{l_{ij}^{0}} a_0^{3/2} \sqrt{\mathscr{G}^b E} \sqrt{2\mathscr{F}_d(\nu, n)} = \frac{\sqrt{\Delta \Gamma_{ij}}}{l_{ij}^{0}} a_0^{3/2} K_{Ic}^b \sqrt{2\mathscr{F}_d(\nu, n)}$$
(10)

where we have used Irwin's formula to relate bond's fracture energy and fracture toughness K_{Ic}^b for mode I fracture: $\mathcal{G}^b = (K_{Ic}^b)^2/E$ [64]. While this may look similar to the classical strength-based crack propagation criteria, it is different in the sense that the critical force is a function of lattice size and is capable of capturing size effect. In fact, the critical bond force in Eq. (10) requires assumptions relating the fracture surface $\Delta\Gamma$ to the length and configuration of bonds within the lattice. Furthermore, expressing the critical force $F_{i,c}^j$ in terms of material fracture energy \mathcal{G}_c or fracture toughness K_{Ic} is only possible by relating the number of broken bonds for the crack to advance one surface unit. Such relationship not only depends on the configuration of material and lattice but also can only be determined by inspection of the simulation box a posteriori (after fracture analysis). Establishing such relationships is relatively straightforward for homogeneous materials and microstructures with simple geometries, but becomes intractable when modeling heterogeneous materials with complex geometries.

Alternatively, the global PMF approach to LEM [54] directly applies the Griffith criteria by removing, sequentially, the material points to create the fracture surface. In the quasi-static formulation of LEM, this manifests itself in the form of breakage of c_i bonds where c_i is the coordination number for node i. Material points, for which the removal would lead to maximum energy release rate in the system will be removed provided that their energy release rate exceeds material fracture energy:

$$k = \arg\max_{k} \quad \mathcal{G}^{k} \ge \mathcal{G}_{c}, \quad \forall k \in \mathcal{N}$$
 (11)

where \mathcal{N} is the set composed of N material points in the lattice and \mathcal{G}^k , the energy release rate corresponding to removal of node k, is given by:

$$\mathcal{G}^k = -\frac{\Pi_k^+ - \Pi_k^-}{\Delta \Gamma^k} \tag{12}$$

with $\Pi_k^- = \sum_{i,j} V_{ij}$ and $\Pi_k^+ = \sum_{i,j \neq k} V_{ij}$ respectively the total energy of the system before and after removal of node k. The fracture surface $\Delta \Gamma^k$ created as a result of removing node k is a_0^2 when the node is connected to an existing defect and $2a_0^2$ otherwise, favoring crack propagation at sites in the vicinity of existing defects. The implementation of global approach allows for direct consideration of Griffith postulate, and since it directly works with material fracture energy \mathcal{G}_c it does not require any assumption to relate the material and bond fracture properties. At every propagation step in a lattice with N material points, the global approach requires N minimization iterations corresponding to relaxing the system after removal of point $k \in \mathcal{N}$ and finding k that lead to maximum energy release rate. As the size of system grows the global approach becomes computationally expensive to the extent that is infeasible to be implemented on large systems. The hybrid approach proposed in this manuscript provides an energy-based alternative for modeling fracture and crack propagation that neither suffers from implementation issues in the local approach nor requires substantial computational cost similar to the global approach.

3. A hybrid PMF approach

We introduce herein a hybrid approach to directly model fracture using the Griffith energy criterion in a computationally efficient manner. The idea behind the proposed approach relies on a postmortem analysis of the results of a fully global approach. It is observed that the points connected to the links with high potential energy are the ones that lead to the maximum energy release rate once removed. This observation is leveraged in the hybrid approach to significantly reduce the dimension of search space when looking for material point k that maximizes the energy release rate.

3.1. High energy bond probing and quasi-static relaxation

At every equilibrium state, i.e. a relaxed system with minimum potential energy, a set \mathcal{L} is formed that includes material points connected to links with energy release rates greater than a threshold $\eta \mathcal{L}_{ii}^b$:

$$\mathcal{L} = \{i, j | \mathcal{L}_{ij} \ge \eta \mathcal{L}_{ij}^b\} \tag{13}$$

where coefficient $\eta > 0$ controls the cardinality of set $\mathscr L$ denoted by ℓ . It is postulated that point k that leads to the highest energy release rate (once removed) lies in this set. The search is then performed within $\mathscr L$ to find material points corresponding to maximum energy release rate while directly applying Griffith fracture criterion for crack propagation, that is : $k = \arg\max_{k \in \mathscr L} \mathscr E^k \ge \mathscr E_c$. As η approaches zero the candidate pool would include all points in the system, $\mathscr L = \mathscr N$, and the hybrid approach will converge to the global approach. For larger values of η close to $\eta_{max} = \max \mathscr E_{ij}/\mathscr E^b_{ij}$, the hybrid approach provides results that are very much akin to the local approach as will be discussed in Section 3.5. Modeling simultaneous propagation of multiple cracks is handled through defining:

$$\varepsilon = \frac{\|\mathcal{G}^{k^*} - \mathcal{G}^k\|}{\mathcal{G}^k} \ll 1, \quad k, k^* \in \mathcal{L}$$
(14)

on the order of simulation error, and removing all nodes in \mathcal{L} with energy release rates close to \mathcal{L}^k . Here \mathcal{L}^k and \mathcal{L}^{k^*} respectively represent the energy release rates when removing points k and k^* . Based on our simulation precision we use $\varepsilon = 0.01$ to ensure round off errors do not impact the selection of crack propagation sites.

Removal of a single or multiple points in the discretized domain will lead to redistribution of forces as the system relaxes leading to subsequent crack growth. This is simulated under a quasi-static condition via formation of a new candidate pool at every propagation step iteratively until the crack propagation stops and the system arrives at a new equilibrium state.

3.2. Computational cost

The computational efficiency of the hybrid approach is directly linked to the choice of η with $\ell \ll N$ as will be discussed in Section 3.5. Fig. 2 compares the computational time of global approach and the hybrid approach for $\eta=0.90$. It is observed that hybrid approach can reduce the computational cost by about two orders of magnitude for moderate-size samples when compared to the global approach. We note that the calculation of system's potential energy requires $\mathcal{O}(N)$ operations. In addition, the CG algorithm typically converges in a fraction of number of variables. That means a maximum of $\mathcal{O}(N^2)$ operations for each relaxation (potential energy minimization) step. Thus the global approach requires a maximum of $\mathcal{O}(N^3)$ operations. This is in contrast to the hybrid approach, which similarly to the local approach, requires $\mathcal{O}(N^2)$ operations. Consistent with the above, on average, the order of operations for global and hybrid approaches shown in Fig. 2 are respectively $\mathcal{O}(N^{2.3})$ and $\mathcal{O}(N^{1.6})$. We finally note that local approach is the most computationally efficient. However, as mentioned above, the implementation of the classical local approach with the cubic lattice is often accompanied with challenges that make it interactable for highly heterogeneous materials.

3.3. Validation

We first validate the hybrid approach by comparing the results obtained for mode I fracture with those in the literature for a notched homogeneous sample subject to triangular displacement as illustrated in Fig. 3a. The material is discretized via a cubic lattice with $n_x = n_y = 50$ and $n_z = 2$. The displacement is incrementally increased to the

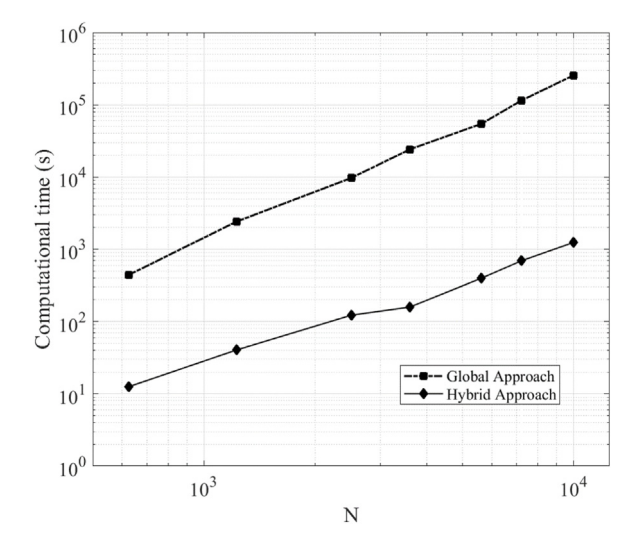


Fig. 2. Computational time for global and hybrid approaches. All simulations are performed on an iMac with Processor Intel(R) Core(TM) i7–6700K CPU 4.00 GHz, 64 GB RAM.

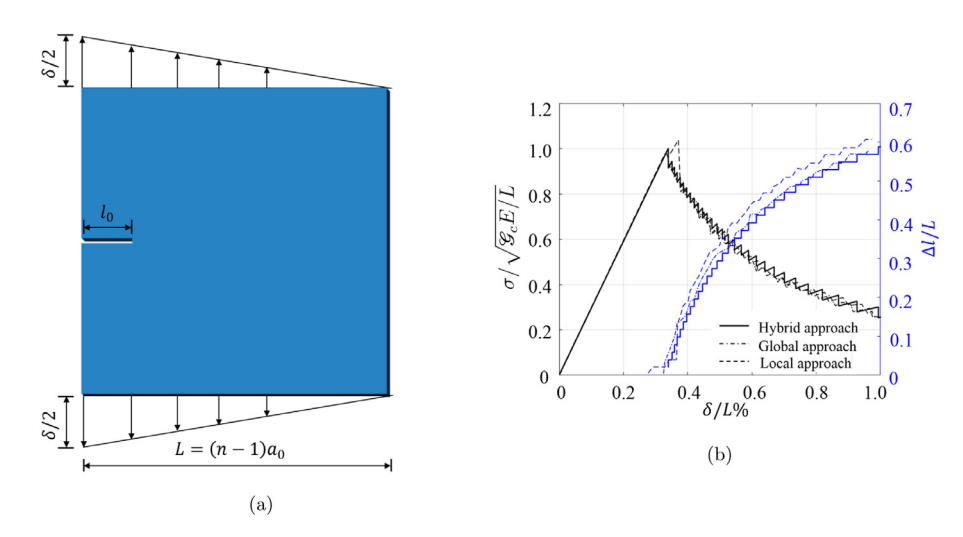


Fig. 3. (a) Notched sample subjected to linear displacement; (b) Comparison of stress–strain (black) and crack-length (blue) obtained from the hybrid approach with $\eta = 0.99$ and those obtained from the local and global approaches [54]. (For interpretation of the references to color in this figure legend, the reader is referred to the web version of this article.)

point of failure. Results obtained via the hybrid approach are compared with those reported in [54] for local and global approaches. The normalized stress–strain curve and the evolution of crack length from the hybrid approach with substantially less computational effort are almost identical to those of the global approach. The stress and strain at the onset of propagation are presented in Figs. 4a and 4b as a function of elastic modulus and material fracture energy. The results show the hybrid approach captures the linear scaling of peak stress with fracture toughness K_c irrespective of elastic modulus. Furthermore, the scaling of peak stress and strain with material fracture energy $\sqrt{\mathcal{G}_c}$ is consistent with the LEFM.

Fig. 5a shows variation of total potential energy and crack growth versus applied strain from the onset of the fracture all the way to complete failure. It is seen that the curve for crack length evolution would converge to a more smooth curve as n increases. Fig. 5b shows variation of total energy of the system as a function of crack length for a sample of fixed size L and for different levels of lattice resolution. The average energy release rate and the J-integral (normalized by material fracture energy), are also plotted in the inset as a function of lattice resolution,

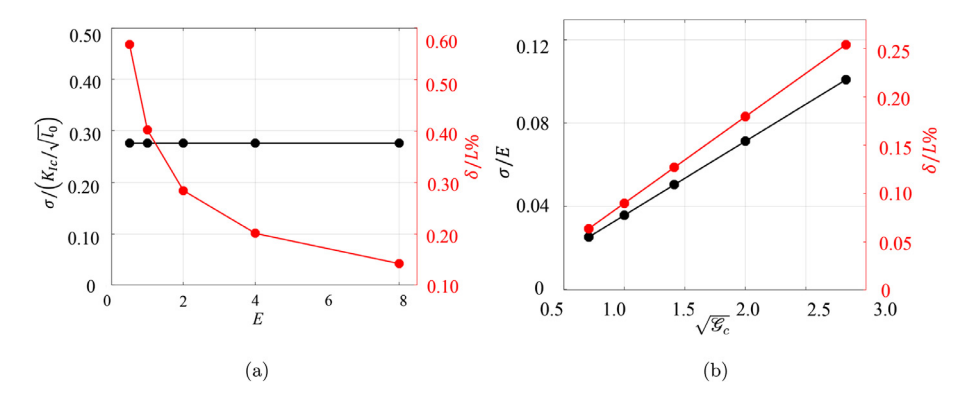


Fig. 4. Variation of stress and strain as a function of (a) elastic modulus E; and (b) fracture energy \mathcal{G}_c .

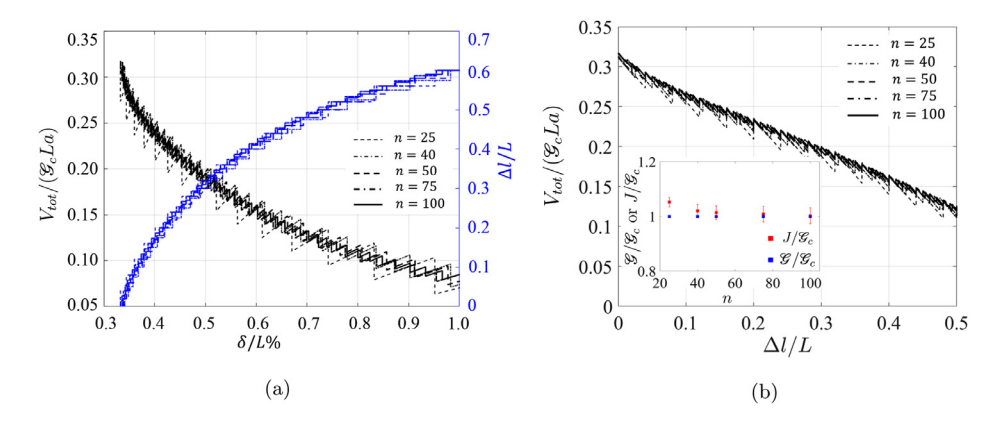


Fig. 5. (a) Total potential energy (black) and crack length (blue) in terms of applied strain (b) total potential energy as a function of crack length for different discretization levels n; the inset shows the energy release rate and J-integral normalized by material fracture energy as a function of n. (For interpretation of the references to color in this figure legend, the reader is referred to the web version of this article.)

with the error bars representing the standard deviation. The average energy release rate \mathcal{G} is obtained according to Eq. (2) and by determining the amount of dissipated energy and the created fracture surface associated with the removed nodes; and the J-integral is calculated according to the classical definition [65]:

$$J = \int_{\partial \mathcal{D}} \left(\frac{1}{2} \left(\underline{\underline{\sigma}} : \underline{\underline{\epsilon}} \right) \left(\underline{\underline{n}} . \underline{\underline{e}_{x}} \right) - \left(\underline{\underline{\sigma}} . \underline{\underline{n}} \right) . \xi_{,x} \right) ds \tag{15}$$

where $\partial \mathcal{D}$ is the contour taken along the boundary of the sample with unit normal \underline{n} , $\underline{e_x}$ is the crack propagation direction, $\xi_{,x}$ is the derivative of displacement with respect to propagation direction, σ is the stress tensor and ϵ is the strain tensor. It can be shown that for the boundary conditions in Fig. 3 the above relation can be simplified as:

$$J = \delta \langle \sigma_{vv} \rangle$$
 (16)

with $\langle \sigma_{yy} \rangle$ the average stress on the boundary in vertical direction [54].

It is seen that, for large enough n, both the energy release rate and the J-integral converge to the fracture energy of the material irrespective of lattice resolution a consequence that is rooted in the use of energy-based criteria for fracture [47,66].

3.4. Size effect

We also examine the hybrid approach as it relates to the deterministic size effect [67]. To this end, we investigate the nominal critical stress, i.e. the stress at the onset of fracture for the notched sample in Fig. 3a for a wide range of sample size ($L_i = 30 - 200$), while keeping the lattice size constant. The initial notch length is $l_0 = L_i/5$ and

X. Wang, M. Botshekan, F.-J. Ulm et al.

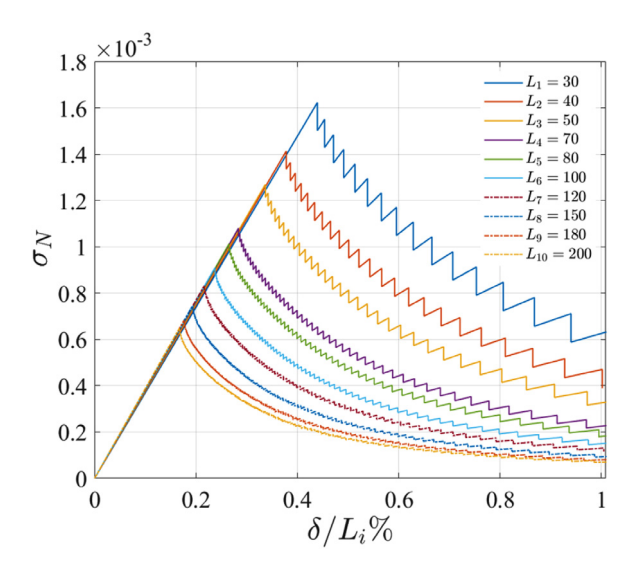


Fig. 6. Stress-strain curve for notched samples of different size L.

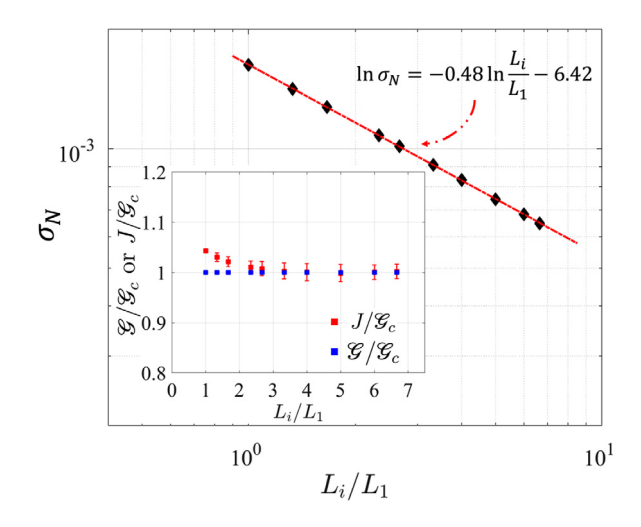


Fig. 7. Nominal stress in terms of sample size. The inset shows the energy release rate and J-integral for different sample sizes.

all samples are subjected to uniaxial linear strain perpendicular to the notch direction. The discretization resolution (lattice size) is kept constant throughout to ensure the same level of singularity at the crack tip. The stress-strain curve in Fig. 6 shows the reduction of nominal stress as the size of sample increases. The nominal stress scales with $L^{-0.48}$, shown in the logarithmic plot in Fig. 7, which is in agreement with LEFM results that indicate a scaling $L^{-0.5}$. The inset in the figure shows the average energy release rate and J-integral in function of sample size. As the sample size increases both J-integral and energy release rate converge to the fracture energy of the material as expected.

We note that one cannot utilize LEFM for modeling fracture of materials with a highly pronounced dissipative zone. However, the PMF approach offers great promise in the modeling of fracture in quasi-brittle or non-brittle materials. This can be done by using non-harmonic potentials and careful calibration of the potential parameters.

3.5. Hand shake with local and global approaches

While the global and local approaches have shown to result in statistically similar fracture behavior [54], they do not produce the same results due to their different propagation criteria and implementation procedure. The

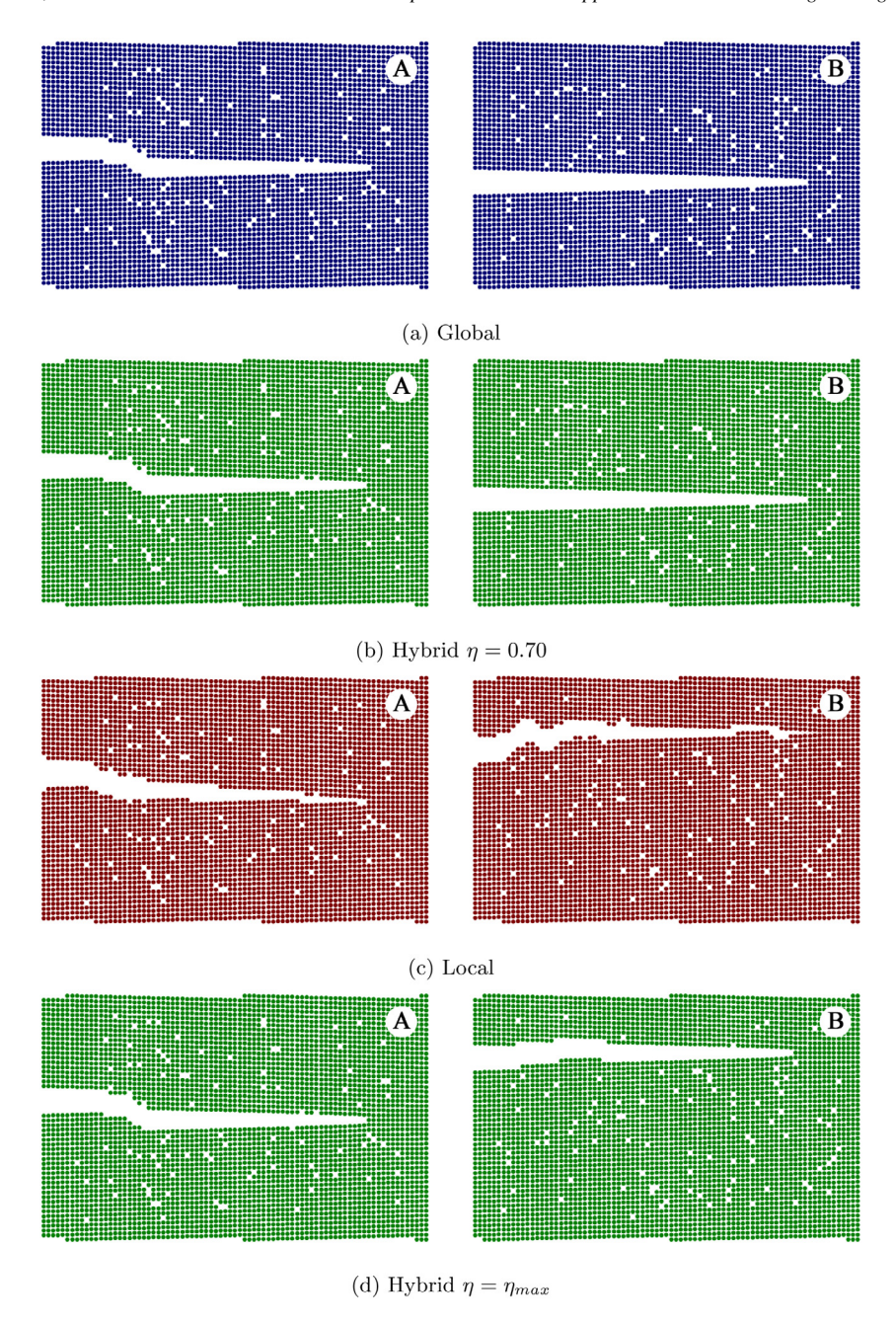


Fig. 8. Crack patterns obtained using (a) global approach; (b) hybrid approach with $\eta = 0.70$; (c) local approach; and (d) hybrid approach with $\eta = 0.99$.

global approach relies on direct and global application of Griffith criteria where a cohort of bonds connected to a material point are removed, whereas the local approach removes bonds with highest stress intensity factor using Irwin fracture criteria to create fracture surface. The hybrid approach offers the best of both worlds; it uses Griffith criterion similar to global approach but localizes the search to points which, if removed, lead to maximum energy release rate. Hence, it is expected that the hybrid approach provides the results that are in between the global and local approaches. This is examined through analysis of a set of heterogeneous, i.e. defective, samples via global, hybrid and local approaches. The heterogeneous samples are generated by random removal of 1.5% of material

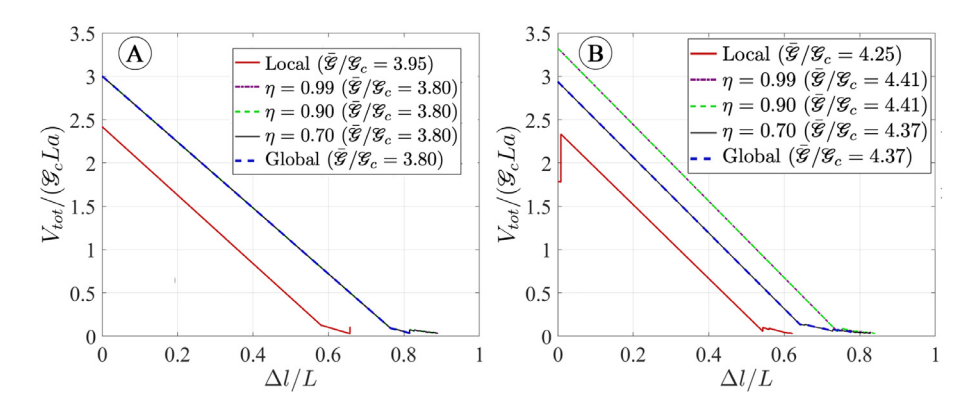


Fig. 9. Normalized total potential energy as a function of crack length. The numbers in the parentheses are the normalized average energy release rate obtained from the slopes of the curves.

points from the initially homogeneous and perfect samples. A linear displacement loading as shown in Fig. 3a with $\delta = 0.01L$ is incrementally applied to the samples. A crack would initiate and then propagate until the energy release rate falls below the fracture energy of the material.

Fig. 8 compares the crack patterns obtained using different approaches for two defective samples. Fig. 8(a) and (c) show the result obtained respectively via global and local approaches, while Fig. 8(b) and (d) present the results using the hybrid approach with different values of η . The crack patterns obtained from different approaches are distinct in samples "B" and similar in sample "A". As η decreases the results of hybrid approach converge to those of the global approach. We observe the hybrid approach with $\eta < 0.7$ predicts crack patterns that are the same as the ones obtained by the global approach, with far less computational expense. The proper choice of η very much depends on heterogeneity in the distribution of stress. Material heterogeneity that determines the number of locations with high stress concentration, for example, is an important factor in the selection of η . Lower values of η are required for highly heterogeneous as they create candidate pools with higher cardinality, and achieve results that are very close or equivalent to the global approach. However, decreasing η beyond a given value will only increase the computational cost with no impact to the accuracy. Large values of η , on the other hand, are expected to generate results that are similar to the local approach, with marginal differences attributed to the removal of bonds with forces above a critical value in the local approach in contrast to the removal of points leading to maximum energy release rate in the hybrid approach; see Fig. 8(c) and (d). Fig. 9 also illustrates the normalized energy as a function of crack extension for the two defective samples shown in Fig. 8 along with the normalized energy release rate. It is seen that the hybrid approach for large values of η and the global approach provide similar results. Furthermore, while the estimated crack length by local approach is smaller (due to its removal of bonds rather than nodes), the critical energy release rates (slope of the energy plots) are similar for all three approaches.

It is worth noting that implementation of the local approach with the cubic lattices shown in Fig. 1 may be challenging due to existence of zero- or compressive-force members at the crack surface that will not break through the application of Irwin fracture criterion. These links will need to be removed a posteriori by accounting for the geometry of crack propagation which would complicate the use of local approach for fracture modeling of heterogeneous materials with complex geometries. This difficulty is circumvented in the hybrid approach that rests on the direct application of global Griffith fracture criteria at a much lower computational expense than that of the global approach.

4. Application to non-homogeneous media

The advantage of the proposed approach is more pronounced in studying crack propagation in heterogeneous materials, where cracks may deflect at the interface between phases or due to presence of pores and defects, propagation may occur along a non-smooth path and material may experience microcracking away from the main crack tip. In fact, allowing the cracks evolve in energetically favorable directions by design, the hybrid approach renders more attractive compared to the continuum approaches for modeling such phenomena and for studying the effective properties of heterogeneous materials. From a variety of fracture toughening mechanisms, in what

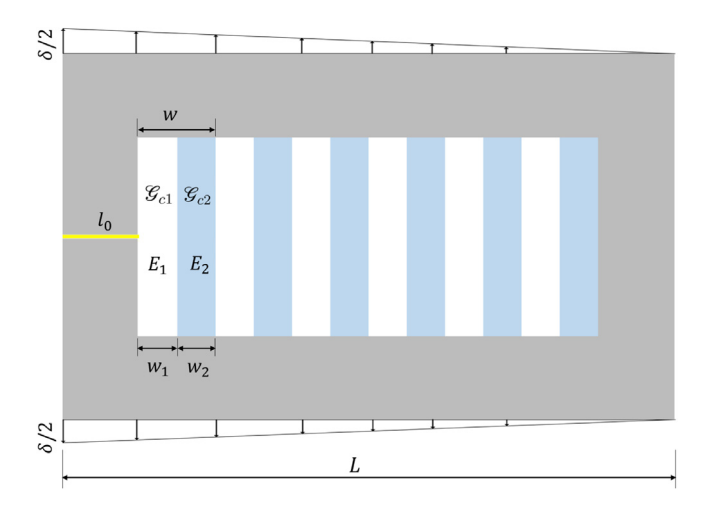


Fig. 10. Two-phase layered composite material subjected to far-field displacement field.

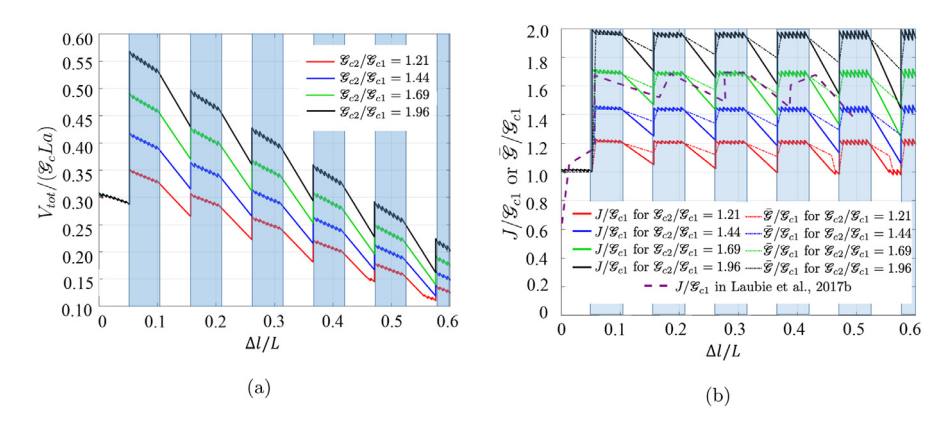


Fig. 11. (a) Variation of total potential energy; (b) J-integral, and energy release rate normalized by \mathcal{G}_{c1} as a function of crack extension. Solid and dash lines represent the normalized J-integral and energy release rate respectively.

follows we focus on elastic modulus and fracture energy heterogeneity, both shown to have great impact on the effective fracture properties at the macroscale [68–70]. More specifically we consider pure mode-I fracture a two-phase periodically layered composite embedded in a homogenized material with effective elastic modulus of the heterogeneous medium subjected to a linear displacement field as shown in Fig. 10.

4.1. Fracture energy heterogeneity

To focus on fracture energy heterogeneity we assume the constituent layers have the same elastic properties $E_1 = E_2 = E$ and different fracture energies $\mathcal{C}_{c2} > \mathcal{C}_{c1}$. Fig. 11(a) illustrates the normalized potential energy as the crack extends through the layered material. The crack propagates in the weaker layer until it is arrested at the interface with the tougher material. As the far field displacement increases providing more energy to the system, the crack would propagate into the tough layer followed by an unstable propagation within the less tough layer. The excess energy needed to overcome the barrier for propagation through the tougher material is indicative of toughening mechanism and the remaining stored energy drives propagation through the weaker material in an unstable manner. Fig. 11(b) shows the variation of energy release rate and J-integral calculated at consecutive equilibrium states. The two values are practically equivalent as we have elastic modulus homogeneity and the J-integral is thus path independent. Using the hybrid approach any propagation of crack is only possible by preserving the thermodynamics of fracture through Griffith criteria in Eq. (1). The energy release rate, thus, fluctuates between

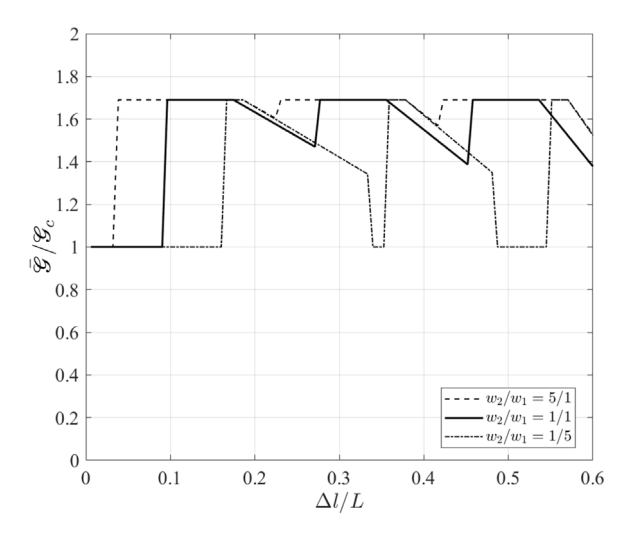


Fig. 12. Normalized energy release rates as a function of crack extension for different volume fraction of constituents ($\mathcal{G}_2/\mathcal{G}_1 = 1.69$).

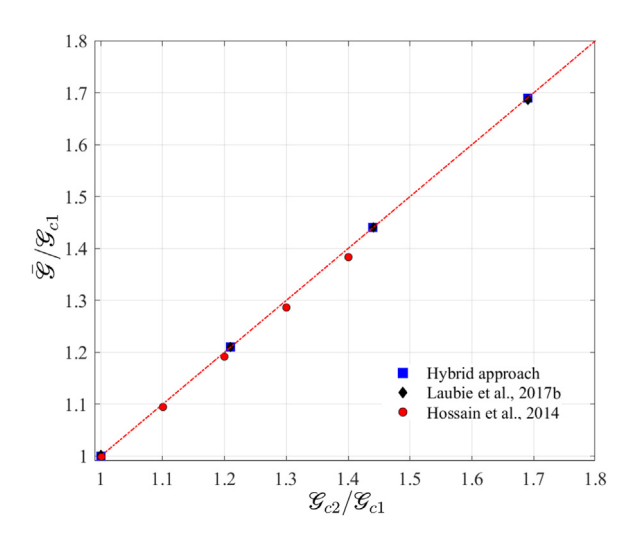


Fig. 13. Normalized macroscopic fracture energy for different values of $\mathcal{G}_{c2}/\mathcal{G}_{c1}$.

fracture energies of the two phases, i.e. $\mathcal{G}_{c1} \leq \bar{\mathcal{G}} \leq \mathcal{G}_{c2}$. The macroscopic fracture energy of the layered composite can be regarded as the maximum J-integral, i.e. the energy release rate of the toughest layer irrespective of the volume fraction of constituents; see Fig. 12. This is consistent with the results reported in literature via different numerical approaches [54,69]; see Fig. 13.

4.2. Elastic modulus heterogeneity

We next consider the constituent layers to have the same fracture energy: $\mathcal{G}_{c1} = \mathcal{G}_{c2} = \mathcal{G}_c$ and vary the elastic modulus of the stiff layer while keeping the elastic modulus of compliant layer constant. While the energy parameters for each constituent are assigned according to calibration equations, the equivalent energy parameters for bonds located in the interface are obtained using the series spring system rule [49] consistent with the Hertzian contact:

$$\frac{2}{\epsilon_{ij}^{n,t(int)}} = \frac{1}{\epsilon_{ij}^{n,t(1)}} + \frac{1}{\epsilon_{ij}^{n,t(2)}}$$
(17)

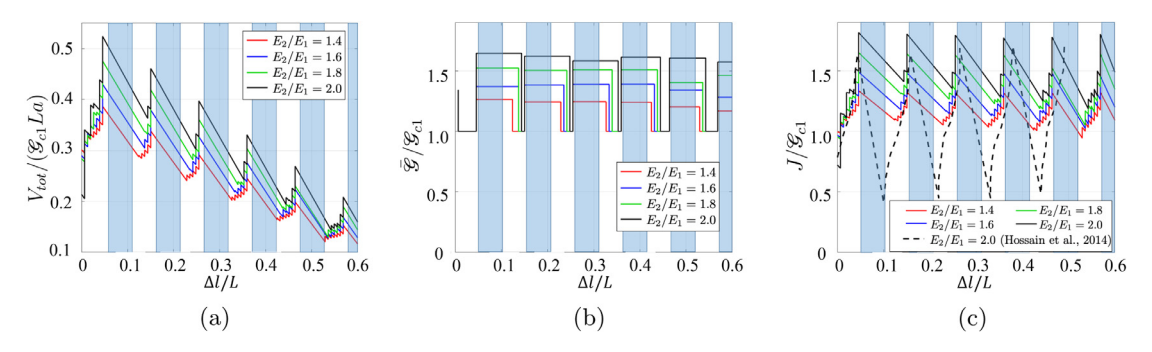


Fig. 14. (a) Normalized total potential energy; (b) energy release rate; and (c) J-integral as a function of normalized crack length.

A linear displacement loading applied incrementally at the boundary of the layered material with an existing notch as illustrated in Fig. 10 is considered. Toughening is observed as crack gets arrested in the compliant region of the composite close to the compliant-stiff material interface. Fig. 14(a) shows, for composites with different elastic modulus contrasts, the normalized total potential energy of the system as the crack propagates. As the crack approaches the interface more external energy is required for propagation through the compliant region and later through the interface. This is consistent with previous observations (see [69]) and can be attributed to the lower stress, and thus driving force experienced by the compliant material when the crack tip is far from the stiff region and the higher driving force needed to deform the stiffer region leading to redistribution of strain energy as the crack approaches the interface. As the crack passes through the stiff region, however, the stress intensity factor increases with scaling of E_2/E_1 while the fracture toughness increases more slowly with scaling $\sqrt{E_2/E_1}$ leading to unstable crack propagation. It is interesting to note that the hybrid approach completely captures this local phenomena albeit using a global energy criterion for crack propagation.

The energy release rate and J-integral at each equilibrium state as crack propagates are also presented in Figs. 14(b,c). The fracture energy is equal to the uniform material fracture energy \mathcal{G}_{c1} in the compliant region where the crack propagation is stable. It then suddenly increases as crack approaches the interface and propagates through the interface and the stiff region in an unstable fashion. Unlike homogeneous materials where the J-integral and energy release rate are in close agreement (see Figs. 5b and 11b) for the case of elastic modulus heterogeneity the J-integral is not path-independent and the results in Figs. 14(c) and (d) do not match. The J-integral is also compared with the results in [69] for $E_2/E_1 = 2$. The differences observed are due to the fact that the semianalytical surfing boundary condition in [69] imposes path-independence of J-integral and its equivalence to the energy release rate even for the case of heterogeneous materials, and the proposed hybrid approach does not [54,70– 72]. Nevertheless, we observe a very close agreement between the maximum value of energy release rate obtained from our hybrid approach and the J-integral given in [69]. The surfing boundary condition also allows for capturing the load-displacement relationship even for the unstable propagation region as the crack passes through the stiff region, that cannot be captured through either load or displacement controlled experiments. Enforcing stability condition is also possible through the addition of controlling terms or viscous dissipation to the numerical scheme (see [73–75]) but is not pursued here since it only provides additional information for regions with low J-integral that are not of interest.

Similar to the case of fracture heterogeneity, for the crack to advance macroscopically, the energy release rate needs to reach its maximum value which can be regarded as the effective fracture energy of the heterogeneous material. An important observation is that the effective fracture energy is an increasing function of the elastic modulus contrast and is "always" greater than the fracture energy of the constituents a clear indication for toughening in the layered composite. Fig. 15 presents the effective energy release rate as a function of elastic modulus contrast showing a close agreement with the results in literature. At small modulus contrasts we observe a linear scaling of normalized energy release rate with elastic modulus ratio which deviates to a nonlinear scaling as E_2/E_1 reaches values greater than 2.63. Crack propagation patterns are also illustrated for different levels of elastic modulus contrast. As observed in Fig. 16(a) the crack propagates smoothly from the compliant region through the stiff region when the elastic modulus contrast is $E_2/E_1 < 2.63$ (region I in Fig. 15). As the elastic modulus contrast increases (region II in Fig. 15) the crack gets arrested close to the compliant-stiff interface in the compliant region while a

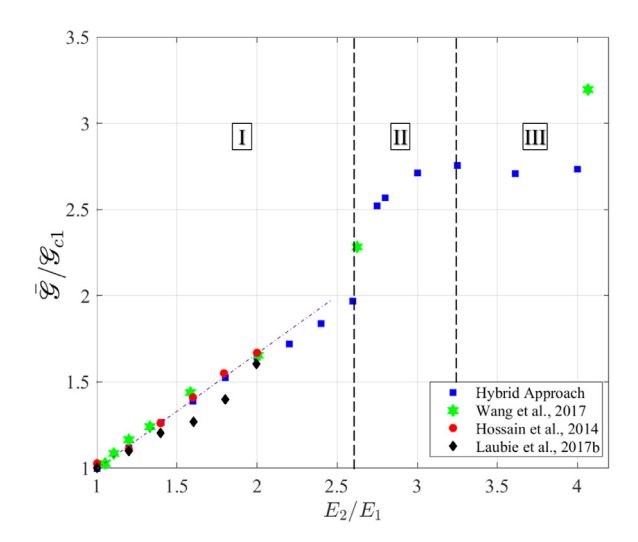


Fig. 15. Normalized energy release rate in terms of elastic modulus contrast E_2/E_1 .

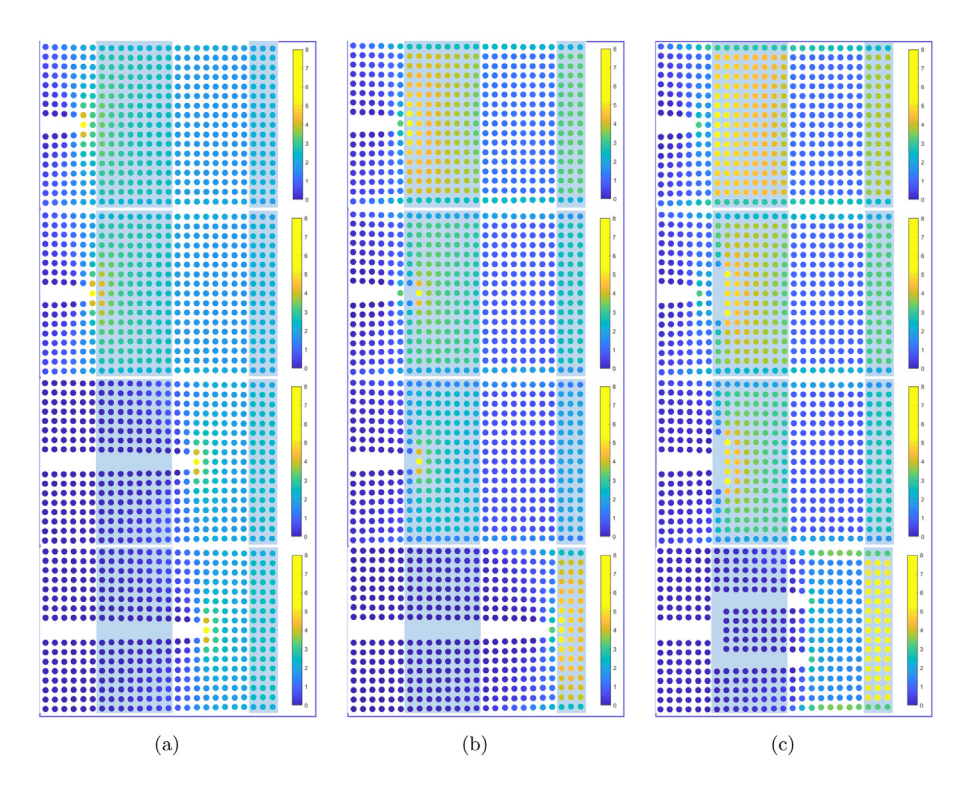


Fig. 16. Crack propagation pattern and normal stress in vertical direction (see Eq. (7)) for the layered material with different elastic modulus contrast (a) $E_2/E_1 = 1.4$, (b) $E_2/E_1 = 3.0$ and (c) $E_2/E_1 = 4$.

new crack nucleates in the stiff region ahead of the original crack. This is attributed to the higher strain energy in the stiff material at the vicinity of the crack compared to the crack tip in compliant region. As a result, the nucleation of a new crack would result in more energy dissipation in comparison with extension of the existing crack within the complaint region. The two cracks soon merge as the propagation continues in an unstable manner (see Fig. 16(b)). This behavior was also observed by [70] at the same range of elastic modulus contrast ($E_2/E_1 > 2.63$). At high contrasts ($E_2/E_1 > 3.30$, region III in Fig. 15) we observe the crack deflecting at the interface before propagating through the stiff material. While this behavior is in agreement with the results reported in literature for large modulus

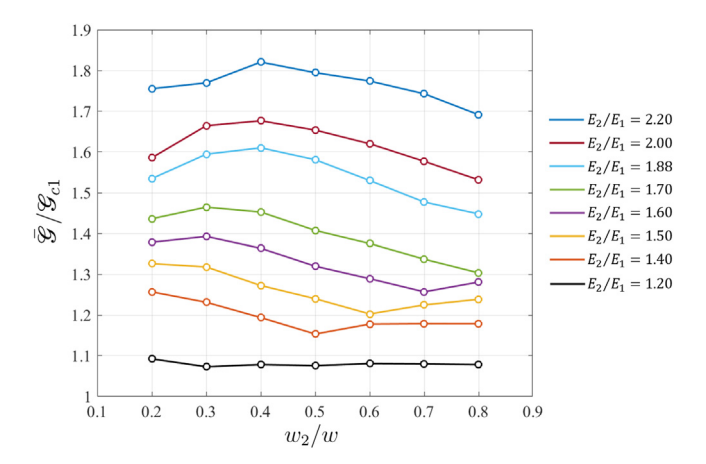


Fig. 17. Macroscopic fracture energy of the material in terms of the volume fraction of the stiff material for different values of elastic modulus contrast.

contrasts [76–78], the corresponding value at which the deflection is observed is higher [76,79]. The difference is attributed to weaker bounding at the interface in our hybrid approach (see Eq. (17)) compared to strong and full bonding in continuum approaches such as the ones used in [70,76], which would lead to different strain energy distribution in the vicinity of the interface. It is expected that adopting a different strategy for assigning potential parameters at the interface than the one used herein (e.g., [49,50,52,61,80,81]) would change the association between ranges of elastic modulus contrast and particular crack propagation patterns.

The impact of volume fraction on effective toughness is illustrated in Fig. 17 for composites with different elastic modulus contrasts. The macroscopic toughness is observed to increase with the modulus contrast due to higher energy needed for crack propagation through the stiff phase. Furthermore, the maximum of macroscopic toughness occurs at materials with larger w_2/w as E_2/E_1 increases. Two competing factors account for fracture toughness variations as the w_2/w increases: (i) maximum value of total energy when the crack approaches the interface and, (ii): fracture surface created in an unstable crack growth. These factors both increase with w_2/w . Higher values of the former increase the fracture toughness, whereas an increase in the latter would lead to reduction of fracture toughness.

4.3. From elastic modulus heterogeneity to toughness anisotropy

The results in Fig. 14(b,c) show how both energy release rate and J-integral increase at the compliant-stiff interface and then decrease at the stiff-compliant interface. This suggests that the effective toughness of heterogeneous materials depends on the direction of the crack propagation. In other words composites with elastic modulus heterogeneity can show anisotropic fracture toughness depending on the gradient of elastic modulus in the direction of crack propagation. To further elucidate this, we examine the fracture properties of two layered composites with elastic modulus heterogeneity and uniform fracture toughness \mathcal{G}_c . The samples are subjected to linear displacement and the elastic moduli of the constituents are selected such that the crack propagates straight without deflection. This way the toughening is attributed only to the elastic modulus heterogeneity. Fig. 18 illustrates the total energy of the system, the effective energy release rate and J-integral for the two samples in function of crack extension. The maximum energy release rate in each sample is observed at the interface with the highest modulus contrast when the crack propagates from a compliant layer to stiffer layer, i.e. the interfaces between layers with elastic moduli $E_1 = 1$ and $E_2 = 1.5$ in sample I and $E_1 = 1$ and $E_4 = 2.5$ in sample II. The higher macroscopic fracture energy observed in sample II due to larger modulus contrast ($\Delta E = 1.5$) in the propagation direction suggests proper placement of layers can be used as a means for effective toughening of the composite at macroscale.

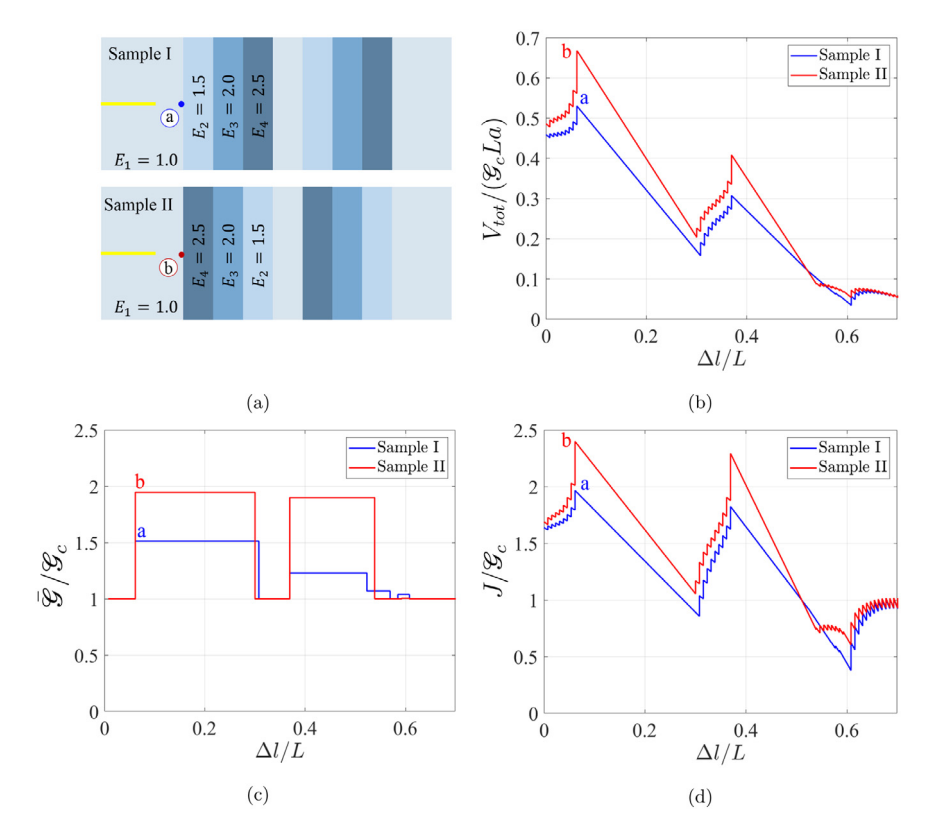


Fig. 18. The impact of elastic modulus gradient on macroscopic fracture properties: (a) the schematic of two samples, (b) normalized total potential energy, (c) average energy release rate, (d) J-integral as a function of crack length.

5. Conclusions

We have developed a hybrid energy-based PMF approach based on LEM for modeling fracture and crack propagation in heterogeneous materials. The proposed approach sequentially removes nodes to create fracture surface by directly applying the Griffith fracture criteria and letting the cracks evolve in energetically favorable directions. The hybrid approach relies on high energy bond probing and relaxation to offer substantially better computational performance with practically the same fidelity in crack path resolution when compared to the global energy approach. Furthermore, it does not suffer from the implementation challenges associated with the local approach both for specific lattice configurations and for evaluating the fracture surface that often render the local approach intractable for heterogeneous materials with complex meso-scale geometries. The proposed approach is validated against the results reported in literature and used to investigate fracture behavior of heterogeneous materials. The following points deserve attention:

- 1. The control parameter η in the proposed approach offers significant flexibility. As η decreases the fracture response captured by the hybrid approach quickly resembles that of the global approach with significantly less computational cost. For large values of η the results are similar to those provided by local approach.
- 2. The energy release rate in a material with fracture energy heterogeneity fluctuates between the fracture energies of the constituent layers. The effective toughness is shown to be the maximum of fracture energies of different layers irrespective of their volume fraction and the direction of crack propagation.
- 3. For layered materials with elastic modulus heterogeneity, the maximum energy release rate occurs when the crack in the compliant region approaches the compliant-stiff interface. Consistent with the literature, we observe a linear scaling between macroscopic toughness and the elastic modulus ratio at small value of modulus contrast ($E_2/E_1 < 2.63$) corresponding to smooth propagation of crack from the compliant phase to the stiff phase. For mid-range modulus contrasts ($2.63 < E_2/E_1 < 3.3$), we observe a monotonically

increasing non-linear relationship between the macroscopic toughness and elastic modulus contrast that is associated with the arrest of the crack tip in the compliant region at the vicinity of the interface and the formation of a new crack in the stiff region. Finally at larger elastic modulus contrasts ($E_2/E_1 > 3.3$), the crack would deflect at the interface before propagating through the stiff material. The upper limit for modulus contrast pertains to the potential parameters at the interface. A spring series relation, consistent with Hertzian contact, results in a lower value compared to the full bonding assumption in continuum approaches.

- 4. In materials with high elastic modulus contrast, the maximum toughness occurs at higher volume fractions of stiff material w_2/w , whereas at low modulus contrasts a lower volume fraction would lead to maximum macroscopic toughness.
- 5. In materials with heterogeneity in elastic modulus, higher fracture toughness can be achieved through arrangement of layers such that the crack tip observes the highest modulus contrast when it travels from the compliant layer to the stiff layer.

Declaration of competing interest

The authors declare that they have no known competing financial interests or personal relationships that could have appeared to influence the work reported in this paper.

Acknowledgments

The authors would like to acknowledge the funding from United States National Science Foundation grant CMMI-2047832 and the support from College of Engineering and Center for Scientific Computing and Visualization Research at the University of Massachusetts Dartmouth.

Appendix. Fracture criterion for harmonic potential in presence of bending

The potential energy considering only the bending interaction potential can be expressed as:

$$V_{ij}^{b} = -\epsilon_{ij}^{0} + \frac{1}{2}\epsilon_{ij}^{t} \left\{ \left(\frac{\delta_{j}^{b} - \delta_{i}^{b}}{l_{ij}^{0}} - \vartheta_{i}^{t} \right)^{2} + \left(\frac{\delta_{j}^{t} - \delta_{i}^{t}}{l_{ij}^{0}} + \vartheta_{i}^{b} \right)^{2} + \left(\frac{\delta_{j}^{b} - \delta_{i}^{b}}{l_{ij}^{0}} - \vartheta_{i}^{t} \right) (\vartheta_{i}^{t} - \vartheta_{j}^{t}) + \left(\frac{\delta_{j}^{t} - \delta_{i}^{t}}{l_{ij}^{0}} - \vartheta_{i}^{b} \right) (\vartheta_{j}^{b} - \vartheta_{i}^{b}) + \left(\frac{\delta_{j}^{t} - \delta_{i}^{t}}{l_{ij}^{0}} - \vartheta_{i}^{b} \right) (\vartheta_{j}^{b} - \vartheta_{i}^{b}) + \frac{1}{3} \left((\vartheta_{j}^{b} - \vartheta_{i}^{b})^{2} + (\vartheta_{i}^{t} - \vartheta_{j}^{t})^{2} \right) \right\}$$

$$(A.1)$$

Taking the derivative of the energy with respect to the corresponding translational or rotational displacement the bonds forces F_i^j and moments M_i^j are expressed as:

$$\vec{F}_{i}^{j} = -\frac{\partial U}{\partial \delta_{i}} = \frac{\epsilon_{ij}^{t}}{l_{ij}^{0}} \left(\frac{\delta_{j}^{b} - \delta_{i}^{b}}{l_{ij}^{0}} - \frac{\vartheta_{j}^{t} - \vartheta_{i}^{t}}{2} \right) \vec{e^{b}} + \frac{\epsilon_{ij}^{t}}{l_{ij}^{0}} \left(\frac{\delta_{j}^{t} - \delta_{i}^{t}}{l_{ij}^{0}} + \frac{\vartheta_{j}^{b} + \vartheta_{i}^{b}}{2} \right) \vec{e^{t}}$$

$$\vec{M}_{i}^{j} = -\frac{\partial U}{\partial \vartheta_{i}} = \frac{\epsilon_{ij}^{t}}{2} \left(\frac{\delta_{j}^{t} - \delta_{i}^{t}}{l_{ij}^{0}} + \frac{\vartheta_{j}^{b} + 3\vartheta_{i}^{b}}{3} \right) \vec{e^{b}} + \frac{\epsilon_{ij}^{t}}{2} \left(\frac{\delta_{j}^{b} - \delta_{i}^{b}}{l_{ij}^{0}} - \frac{\vartheta_{j}^{t} + 3\vartheta_{i}^{t}}{3} \right) \vec{e^{t}}$$
(A.2)

The above is used to express the deformations δ_i^b , δ_i^t , ϑ_i^b and ϑ_i^t in functions of bonds forces and moments. Subsequent substitution into the energy expression in (A.1) will lead to:

$$V_{ij}^{b} = -\epsilon_{ij}^{0} + \frac{2}{\epsilon_{ij}^{t}} \left\{ (M_{j}^{i})^{2} + (M_{i}^{j})^{2} - (M_{j}^{i}M_{i}^{j}) \right\}$$
(A.3)

where we have also used the elastic equilibrium in (6). For the general case where both stretch and bending actions are present the superposed potential energy reads:

$$V_{ij} = -\epsilon_{ij}^0 + \frac{(l_{ij}^0 F_i^j)^2}{2\epsilon_{ij}^n} + \frac{2}{\epsilon_{ij}^t} \left((M_j^i)^2 + (M_i^j)^2 - (M_j^i M_i^j) \right)$$
(A.4)

Once the bond breaks the energy in the bond is dissipated into heat $(V_{ij} = 0)$. The fracture criterion thus reads:

$$\frac{(l_{ij}^{0}F_{j}^{i})^{2}}{2\epsilon_{ii}^{n}} + \frac{2}{\epsilon_{ii}^{t}} \left((M_{j}^{i})^{2} + (M_{i}^{j})^{2} - (M_{j}^{i}M_{i}^{j}) \right) \leq \mathcal{G}^{b} d\Gamma_{ij}$$
(A.5)

References

- [1] H. Gao, B. Ji, I.L. Jäger, E. Arzt, P. Fratzl, Materials become insensitive to flaws at nanoscale: lessons from nature, Proc. Natl. Acad. Sci. 100 (10) (2003) 5597–5600, http://dx.doi.org/10.1073/pnas.0631609100.
- [2] P. Fratzl, R. Weinkamer, Nature's hierarchical materials, Prog. Mater. Sci. 52 (8) (2007) 1263–1334, http://dx.doi.org/10.1016/j.pmatsci. 2007.06.001.
- [3] E. Munch, M.E. Launey, D.H. Alsem, E. Saiz, A.P. Tomsia, R.O. Ritchie, Tough, bio-inspired hybrid materials, Science 322 (5907) (2008) 1516–1520, http://dx.doi.org/10.1126/science.1164865.
- [4] R. Affes, J.Y. Delenne, Y. Monerie, F. Radjaï, V. Topin, Tensile strength and fracture of cemented granular aggregates, Eur. Phys. J. E (2012) http://dx.doi.org/10.1140/epje/i2012-12117-7.
- [5] X. Li, Z. Liu, S. Cui, C. Luo, C. Li, Z. Zhuang, Predicting the effective mechanical property of heterogeneous materials by image based modeling and deep learning, Comput. Methods Appl. Mech. Engrg. (2019) http://dx.doi.org/10.1016/j.cma.2019.01.005.
- [6] S. Torquato, H. Haslach Jr, Random heterogeneous materials: microstructure and macroscopic properties, Appl. Mech. Rev. 55 (4) (2002) B62–B63, http://dx.doi.org/10.1115/1.1483342.
- [7] C. González, J. Segurado, J. Llorca, Numerical simulation of elasto-plastic deformation of composites: evolution of stress microfields and implications for homogenization models, J. Mech. Phys. Solids 52 (7) (2004) 1573–1593, http://dx.doi.org/10.1016/j.jmps.2004.01.002.
- [8] N. Charalambakis, Homogenization techniques and micromechanics. A survey and perspectives, Appl. Mech. Rev. 63 (3) (2010) http://dx.doi.org/10.1115/1.4001911.
- [9] F. Barthelat, R. Rabiei, Toughness amplification in natural composites, J. Mech. Phys. Solids 59 (4) (2011) 829–840, http://dx.doi.org/ 10.1016/j.jmps.2011.01.001.
- [10] O. Tamate, The effect of a circular inclusion on the stresses around a line crack in a sheet under tension, Int. J. Fract. Mech. (1968) http://dx.doi.org/10.1007/BF00185261.
- [11] C. Atkinson, The interaction between a crack and an inclusion, Internat. J. Engrg. Sci. (1972) http://dx.doi.org/10.1016/0020-7225(72)90011-0.
- [12] H. Tada, P.C. Paris, G.R. Irwin, The stress analysis of cracks, in: Handbook, Vol. 34, Del Research Corporation, 1973.
- [13] F. Erdogan, G.D. Gupta, M. Ratwani, Interaction between a circular inclusion and an arbitrarily oriented crack, J. Appl. Mech. Trans. ASME (1974) http://dx.doi.org/10.1115/1.3423424.
- [14] F. Erdogan, G.D. Gupta, The inclusion problem with a crack crossing the boundary, Int. J. Fract. (1975) http://dx.doi.org/10.1007/ BF00034709.
- [15] M.-C. Lu, F. Erdogan, Stress intensity factors in two bonded elastic layers containing cracks perpendicular to and on the interface-I. Analysis, Eng. Fract. Mech. (1983) http://dx.doi.org/10.1016/0013-7944(83)90045-0.
- [16] M.H. Santare, L.M. Keer, Interaction between an edge dislocation and a rigid elliptical inclusion, J. Appl. Mech. Trans. ASME (1986) http://dx.doi.org/10.1115/1.3171768.
- [17] N. Aravas, R.M. McMeeking, Finite element analysis of void growth near a blunting crack tip, J. Mech. Phys. Solids (1985) http://dx.doi.org/10.1016/0022-5096(85)90020-1.
- [18] P.G. Charalambides, R.M. McMeeking, Finite element method simulation of crack propagation in a brittle microcracking solid, Mech. Mater. (1987) http://dx.doi.org/10.1016/0167-6636(87)90023-8.
- [19] Z.H. Kassam, R.J. Zhang, Z. Wang, Finite element simulation to investigate interaction between crack and particulate reinforcements in metal-matrix composites, Mater. Sci. Eng. A (1995) http://dx.doi.org/10.1016/0921-5093(95)09828-3.
- [20] M. Vaz Jr, D. Owen, Aspects of ductile fracture and adaptive mesh refinement in damaged elasto-plastic materials, Internat. J. Numer. Methods Engrg. 50 (1) (2001) 29–54, http://dx.doi.org/10.1002/1097-0207(20010110)50:1<29::AID-NME18>3.0.CO;2-G.
- [21] F.M. Andrade Pires, E.A. de Souza Neto, D.R. Owen, On the finite element prediction of damage growth and fracture initiation in finitely deforming ductile materials, Comput. Methods Appl. Mech. Engrg. (2004) http://dx.doi.org/10.1016/j.cma.2004.01.038.
- [22] I. Babuška, W.C. Rheinboldt, A-posteriori error estimates for the finite element method, Internat. J. Numer. Methods Engrg. 12 (10) (1978) 1597–1615, http://dx.doi.org/10.1002/nme.1620121010.
- [23] O.C. Zienkiewicz, J.Z. Zhu, A simple error estimator and adaptive procedure for practical engineering analysis, Internat. J. Numer. Methods Engrg. 24 (2) (1987) 337–357, http://dx.doi.org/10.1002/nme.1620240206.
- [24] S.E. Benzley, Representation of singularities with isoparametric finite elements, Internat. J. Numer. Methods Engrg. (1974) http://dx.doi.org/10.1002/nme.1620080310.
- [25] J.M. Melenk, I. Babuška, The partition of unity finite element method: Basic theory and applications, Comput. Methods Appl. Mech. Engrg. (1996) http://dx.doi.org/10.1016/S0045-7825(96)01087-0.
- [26] T. Belytschko, T. Black, Elastic crack growth in finite elements with minimal remeshing, Internat. J. Numer. Methods Engrg. (1999) http://dx.doi.org/10.1002/(SICI)1097-0207(19990620)45:5<601::AID-NME598>3.0.CO;2-S.
- [27] N. Moës, J. Dolbow, T. Belytschko, A finite element method for crack growth without remeshing, Internat. J. Numer. Methods Engrg. (1999) http://dx.doi.org/10.1002/(SICI)1097-0207(19990910)46:1<131::AID-NME726>3.0.CO;2-J.
- [28] M. Jirásek, Comparative study on finite elements with embedded discontinuities, Comput. Methods Appl. Mech. Engrg. (2000) http://dx.doi.org/10.1016/S0045-7825(99)00154-1.

- [29] N. Sukumar, D.L. Chopp, N. Moës, T. Belytschko, Modeling holes and inclusions by level sets in the extended finite-element method, Comput. Methods Appl. Mech. Engrg. (2001) http://dx.doi.org/10.1016/S0045-7825(01)00215-8.
- [30] N. Moës, M. Cloirec, P. Cartraud, J.F. Remacle, A computational approach to handle complex microstructure geometries, Comput. Methods Appl. Mech. Engrg. (2003) http://dx.doi.org/10.1016/S0045-7825(03)00346-3.
- [31] A. Hansbo, P. Hansbo, A finite element method for the simulation of strong and weak discontinuities in solid mechanics, Comput. Methods Appl. Mech. Engrg. (2004) http://dx.doi.org/10.1016/j.cma.2003.12.041.
- [32] J. Oliver, A.E. Huespe, P.J. Sánchez, A comparative study on finite elements for capturing strong discontinuities: E-FEM vs X-FEM, Comput. Methods Appl. Mech. Engrg. (2006) http://dx.doi.org/10.1016/j.cma.2005.09.020.
- [33] F. Riccardi, E. Kishta, B. Richard, A step-by-step global crack-tracking approach in E-FEM simulations of quasi-brittle materials, Eng. Fract. Mech. (2017) http://dx.doi.org/10.1016/j.engfracmech.2016.11.032.
- [34] T.P. Fries, T. Belytschko, The intrinsic XFEM: A method for arbitrary discontinuities without additional unknowns, Internat. J. Numer. Methods Engrg. (2006) http://dx.doi.org/10.1002/nme.1761.
- [35] N. Sukumar, J.E. Dolbow, N. Moës, Extended finite element method in computational fracture mechanics: a retrospective examination, Int. J. Fract. (2015) http://dx.doi.org/10.1007/s10704-015-0064-8.
- [36] P.D. Beale, D.J. Srolovitz, Elastic fracture in random materials, Phys. Rev. B (1988) http://dx.doi.org/10.1103/PhysRevB.37.5500.
- [37] W.A. Curtin, H. Scher, Brittle fracture in disordered materials: A spring network model, J. Mater. Res. (1990) http://dx.doi.org/10. 1557/JMR.1990.0535.
- [38] G. Cusatis, D. Pelessone, A. Mencarelli, Lattice discrete particle model (LDPM) for failure behavior of concrete. I: Theory, in: Cement and Concrete Composites, 2011, http://dx.doi.org/10.1016/j.cemconcomp.2011.02.011.
- [39] L. Scholtès, F.V. Donzé, A DEM model for soft and hard rocks: Role of grain interlocking on strength, J. Mech. Phys. Solids (2013) http://dx.doi.org/10.1016/j.jmps.2012.10.005.
- [40] S.G. Psakhie, E.V. Shilko, A.S. Grigoriev, S.V. Astafurov, A.V. Dimaki, A.Y. Smolin, A mathematical model of particle-particle interaction for discrete element based modeling of deformation and fracture of heterogeneous elastic-plastic materials, Eng. Fract. Mech. (2014) http://dx.doi.org/10.1016/j.engfracmech.2014.04.034.
- [41] A. Abdelaziz, Q. Zhao, G. Grasselli, Grain based modelling of rocks using the combined finite-discrete element method, Comput. Geotech. (2018) http://dx.doi.org/10.1016/j.compgeo.2018.07.003.
- [42] E. Schlangen, E.J. Garboczi, Fracture simulations of concrete using lattice models: computational aspects, Eng. Fract. Mech. (1997) http://dx.doi.org/10.1016/s0013-7944(97)00010-6.
- [43] V. Topin, J.Y. Delenne, F. Radjai, L. Brendel, F. Mabille, Strength and failure of cemented granular matter, Eur. Phys. J. E (2007) http://dx.doi.org/10.1140/epje/i2007-10201-9.
- [44] M. Nikolić, X.N. Do, A. Ibrahimbegovic, Ž. Nikolić, Crack propagation in dynamics by embedded strong discontinuity approach: Enhanced solid versus discrete lattice model, Comput. Methods Appl. Mech. Engrg. 340 (2018) 480–499, http://dx.doi.org/10.1016/j.cma.2018.06.012.
- [45] M. Nikolić, E. Karavelić, A. Ibrahimbegovic, P. Miščević, Lattice element models and their peculiarities, Arch. Comput. Methods Eng. (2018) http://dx.doi.org/10.1007/s11831-017-9210-y.
- [46] A. Hrennikoff, Solution of problems of elasticity by the frame-work method, Appl. Sci. Res. (1941) http://dx.doi.org/10.1115/1.4009129.
- [47] Z. Pan, R. Ma, D. Wang, A. Chen, A review of lattice type model in fracture mechanics: theory, applications, and perspectives, Eng. Fract. Mech. (2018) http://dx.doi.org/10.1016/j.engfracmech.2017.12.037.
- [48] H. Herrmann, Introduction to modern ideas on fracture patterns, in: Random Fluctuations and Pattern Growth: Experiments and Models, A, 1988, pp. 149–160, Ch. A. URL https://doi.org/10.1007/978-94-009-2653-0_27.
- [49] M. Ostoja-Starzewski, Lattice models in micromechanics, Appl. Mech. Rev. (2002) http://dx.doi.org/10.1115/1.1432990.
- [50] M. Ostoja-Starzewski, P.Y. Sheng, K. Alzebdeh, Spring network models in elasticity and fracture of composites and polycrystals, Comput. Mater. Sci. (1996) http://dx.doi.org/10.1016/s0927-0256(96)00064-x.
- [51] A. Arslan, R. Ince, B.L. Karihaloo, Improved lattice model for concrete fracture, J. Eng. Mech. (2002) http://dx.doi.org/10.1061/(ASCE) 0733-9399(2002)128:1(57).
- [52] B.L. Karihaloo, P.F. Shao, Q.Z. Xiao, Lattice modelling of the failure of particle composites, Eng. Fract. Mech. (2003) http://dx.doi.org/10.1016/S0013-7944(03)00004-3.
- [53] A.A. Griffith, The phenomena of rupture and flow in solids, Phil. Trans. R. Soc. A (1921) http://dx.doi.org/10.1098/rsta.1921.0006, arXiv:arXiv:1011.1669v3.
- [54] H. Laubie, F. Radjaï, R. Pellenq, F.-J. Ulm, A potential-of-mean-force approach for fracture mechanics of heterogeneous materials using the lattice element method, J. Mech. Phys. Solids 105 (2017) 116–130, http://dx.doi.org/10.1016/j.jmps.2017.05.006.
- [55] J. Aqvist, Ion-water interaction potentials derived from free energy perturbation simulations, J. Phys. Chem. 94 (21) (1990) 8021–8024, http://dx.doi.org/10.1021/j100384a009.
- [56] K. Ioannidou, K.J. Krakowiak, M. Bauchy, C.G. Hoover, E. Masoero, S. Yip, F.-J. Ulm, P. Levitz, R.J.-M. Pellenq, E. Del Gado, Mesoscale texture of cement hydrates, Proc. Natl. Acad. Sci. (2016) http://dx.doi.org/10.1073/pnas.1520487113.
- [57] E. Schlangen, E.J. Garboczi, New method for simulating fracture using an elastically uniform random geometry lattice, Internat. J. Engrg. Sci. (1996) http://dx.doi.org/10.1016/0020-7225(96)00019-5.
- [58] H. Laubie, S. Monfared, F. Radjaï, R. Pellenq, F.-J. Ulm, Effective potentials and elastic properties in the Lattice-element method: Isotropy and transverse isotropy, J. Nanomech. Micromech. (2017) http://dx.doi.org/10.1061/(ASCE)NM.2153-5477.0000125.
- [59] R. Fletcher, Function minimization by conjugate gradients, Comput. J. (1964) http://dx.doi.org/10.1093/comjnl/7.2.149.
- [60] J. Nocedal, S.J. Wright, Numerical optimization 2nd edition, in: International ADAMS User Conference, Springer, New York, 2000, http://dx.doi.org/10.1007/BF01068601, Ch. 5.

- [61] E. Schlangen, J.G. van Mier, Experimental and numerical analysis of micromechanisms of fracture of cement-based composites, Cem. Concr. Compos. (1992) http://dx.doi.org/10.1016/0958-9465(92)90004-F.
- [62] E. Schalangen, Experimental and numerical analysis of fracture process in concrete, Heron (1993).
- [63] J.G. Van Mier, Fracture Processes of Concrete: Assessment of Material Parameters for Fracture Models, 2017, http://dx.doi.org/10. 1201/b22384.
- [64] G.R. Irwin, Fracture, in: S. Flügge (Ed.), Elasticity and Plasticity / Elastizität und Plastizität, Springer Berlin Heidelberg, Berlin, Heidelberg, 1958, pp. 551–590, URL https://doi.org/10.1007/978-3-662-43081-1_5.
- [65] J. Rice, P. Paris, J. Merkle, Some further results of J-integral analysis and estimates, in: Progress in Flaw Growth and Fracture Toughness Testing, ASTM International, 1973, pp. 231–245, http://dx.doi.org/10.1520/STP49643S.
- [66] M. Mungule, B.K. Raghuprasad, Meso-scale studies in fracture of concrete: A numerical simulation, in: Computers and Structures, 2011, http://dx.doi.org/10.1016/j.compstruc.2011.02.007.
- [67] Z.P. Bažant, Size effect on structural strength: A review, Arch. Appl. Mech. (1999) http://dx.doi.org/10.1007/s004190050252, arXiv: arXiv:1011.1669v3.
- [68] H. Gao, Fracture analysis of nonhomogeneous materials via a moduli-perturbation approach, Int. J. Solids Struct. (1991) http://dx.doi.org/10.1016/0020-7683(91)90068-Q.
- [69] M.Z. Hossain, C.J. Hsueh, B. Bourdin, K. Bhattacharya, Effective toughness of heterogeneous media, J. Mech. Phys. Solids (2014) http://dx.doi.org/10.1016/j.jmps.2014.06.002.
- [70] N. Wang, S. Xia, Cohesive fracture of elastically heterogeneous materials: An integrative modeling and experimental study, J. Mech. Phys. Solids (2017) http://dx.doi.org/10.1016/j.jmps.2016.09.004.
- [71] N. Simha, F. Fischer, O. Kolednik, C. Chen, Inhomogeneity effects on the crack driving force in elastic and elastic-plastic materials, J. Mech. Phys. Solids 51 (1) (2003) 209–240, http://dx.doi.org/10.1016/S0022-5096(02)00025-X.
- [72] O. Kolednik, J. Predan, G. Shan, N. Simha, F.D. Fischer, On the fracture behavior of inhomogeneous materials—A case study for elastically inhomogeneous bimaterials, Int. J. Solids Struct. 42 (2) (2005) 605–620, http://dx.doi.org/10.1016/j.ijsolstr.2004.06.064.
- [73] Y.F. Gao, A.F. Bower, A simple technique for avoiding convergence problems in finite element simulations of crack nucleation and growth on cohesive interfaces, Modelling Simulation Mater. Sci. Eng. (2004) http://dx.doi.org/10.1088/0965-0393/12/3/007.
- [74] S.M. Xia, Y.F. Gao, A.F. Bower, L.C. Lev, Y.T. Cheng, Delamination mechanism maps for a strong elastic coating on an elastic-plastic substrate subjected to contact loading, Int. J. Solids Struct. (2007) http://dx.doi.org/10.1016/j.ijsolstr.2006.10.009.
- [75] L. Hamitouche, M. Tarfaoui, A. Vautrin, An interface debonding law subject to viscous regularization for avoiding instability: Application to the delamination problems, Eng. Fract. Mech. (2008) http://dx.doi.org/10.1016/j.engfracmech.2007.12.014.
- [76] M.-Y. He, J.W. Hutchinson, Crack deflection at an interface between dissimilar elastic materials, Int. J. Solids Struct. (1989) http://dx.doi.org/10.1016/0020-7683(89)90021-8.
- [77] M.Y. He, A.G. Evans, J.W. Hutchinson, Crack deflection at an interface between dissimilar elastic materials: Role of residual stresses, Int. J. Solids Struct. (1994) http://dx.doi.org/10.1016/0020-7683(94)90025-6.
- [78] D. Leguillon, C. Lacroix, E. Martin, Interface debonding ahead of a primary crack, J. Mech. Phys. Solids 48 (10) (2000) 2137–2161, http://dx.doi.org/10.1016/S0022-5096(99)00101-5.
- [79] D. Martínez, V. Gupta, Energy criterion for crack deflection at an interface between two orthotropic media, J. Mech. Phys. Solids (1994) http://dx.doi.org/10.1016/0022-5096(94)90034-5.
- [80] J.G. Van Mier, M.R. Van Vliet, Influence of microstructure of concrete on size/scale effects in tensile fracture, Eng. Fract. Mech. (2003) http://dx.doi.org/10.1016/S0013-7944(02)00222-9.
- [81] G. Lilliu, J.G. van Mier, 3D lattice type fracture model for concrete, Eng. Fract. Mech. (2003) http://dx.doi.org/10.1016/S0013-7944(02)00158-3.